Published in final edited form as:

Cell Mol Bioeng. 2015 March ; 8(1): 160–177. doi:10.1007/s12195-014-0370-7.

Polarized actin structural dynamics in response to cyclic uniaxial stretch

Lawrence Huang[1,*] and **Brian P. Helmke**[1,2]

[1]Department of Biomedical Engineering, University of Virginia, P. O. Box 800759, Charlottesville, Virginia 22908

[2]Robert M. Berne Cardiovascular Research Center, University of Virginia, P. O. Box 800759, Charlottesville, Virginia 22908

Abstract

Endothelial cell (EC) alignment to directional flow or stretch supports anti-inflammatory functions, but mechanisms controlling polarized structural adaptation in response to physical cues remain unclear. This study aimed to determine whether factors associated with early actin edge ruffling implicated in cell polarization are prerequisite for stress fiber (SF) reorientation in response to cyclic uniaxial stretch. Time-lapse analysis of EGFP-actin in confluent ECs showed that onset of either cyclic uniaxial or equibiaxial stretch caused a non-directional increase in edge ruffling. Edge activity was concentrated in a direction perpendicular to the stretch axis after 60 min, consistent with the direction of SF alignment. Rho-kinase inhibition caused reorientation of both stretch-induced edge ruffling and SF alignment parallel to the stretch axis. Arp2/3 inhibition attenuated stretch-induced cell elongation and disrupted polarized edge dynamics and microtubule organizing center reorientation, but it had no effect on the extent of SF reorientation. Disrupting localization of p21-activated kinase (PAK) did not prevent stretch-induced SF reorientation, suggesting that this Rac effector is not critical in regulating stretch-induced cytoskeletal remodeling. Overall, these results suggest that directional edge ruffling is not a primary mechanism that guides SF reorientation in response to stretch; the two events are coincident but not causal.

Key Terms

mechanotransduction; endothelial cell; planar cell polarity; substrate strain

Introduction

Endothelial cells (ECs) in vivo are constantly subjected to hemodynamic forces such as shear stress and cyclic strain that result from pulsatile blood flow and circumferential and

Address for correspondence: Brian P. Helmke, Ph.D., Department of Biomedical Engineering, University of Virginia, P. O. Box 800759, Charlottesville, VA 22908, Tel. +1 434-924-1726, Fax +1 434-982-3870, helmke@virginia.edu.

*Current address: Lawrence Huang, Ph.D., Department of Surgery, University of California, San Francisco, San Francisco, CA 94143

Lawrence Huang and Brian P. Helmke declare that they have no conflicts of interest.

No human studies were carried out by the authors for this article. No animal studies were carried out by the authors for this article.

longitudinal deformation of the vessel wall. The local mechanical environment plays an important role in regulating EC structure and function. In straight sections of arteries that are characterized by unidirectional laminar flow and uniaxial circumferential strain, ECs are elongated and align parallel to the direction of flow and perpendicular to the principle axis of stretch, a morphology which has been linked to an atheroprotective phenotype. Cytoskeletal filaments in these cells are oriented parallel to the axis of elongation.[3] In contrast, ECs in regions of arterial bifurcations or high curvature with a small net forward flow component and no clear stretch axis adopt a polygonal, cobblestone morphology with random cytoskeletal filament orientations.[3] These sites of disturbed hemodynamics correlate with the focal pattern of atherogenesis.[39,45] Consistent with cell and cytoskeletal alignment, shear stress and cyclic strain enhance EC migration parallel to the flow direction[31] and perpendicular to the stretch axis,[33] respectively. These results demonstrate that external physical cues induce spatially polarized EC adaptation.

During the initial stages of polarization, cells actively probe the composition and rigidity of the extracellular matrix (ECM) by extending actin-rich lamellipodia and edge ruffles in search of spatial cues. For example, a step increase in shear stress causes a transient increase in non-directional actin edge ruffling and area expansion in subconfluent ECs that peaks after 12–15 min and then subsides. By 10–15 min, lamellipodium formation occurs preferentially in the downstream direction and coincides with the formation of new focal complexes and with cell migration.[4,29,34] The location and time scale of edge ruffling is consistent with that of Rac activation by flow.[42] Thus, force-induced spatial asymmetry of actin polymerization at cell edges at this early time scale may represent an active mechanosensing response that guides the establishment of planar cell polarity.[44]

While it is established that cyclic uniaxial stretch causes perpendicular alignment of ECs over a time scale of hours,[3,25] mechanisms controlling cell polarization in response to ECM stretch have not been elucidated. Static (constant magnitude) equibiaxial stretch inhibits edge ruffling in subconfluent vascular smooth muscle cells within minutes through global deactivation of Rac, whereas static uniaxial stretch causes increased lamellipodium extension at the ends of the cells and decreased extension along the stretched sides of cells through vectorial deactivation of Rac.[24] In contrast to static stretch, onset of either cyclic uniaxial or equibiaxial stretch triggers increased edge ruffling in ECs within minutes, consistent with responses to onset of shear stress.[19] In subconfluent fibroblasts, although Rac activity remains constant during the first 30 min of cyclic uniaxial stretch, edge protrusion activity perpendicular to stretch increases and protrusion activity parallel to stretch decreases over an alignment time scale of 3 h.[7] Together with the observation that constitutively active V12Rac blocks stretch-induced stress fiber (SF) alignment,[24] these results suggest that rapid edge dynamics, which are mediated by Rac, may contribute to SF reorientation at later time scales.

A causal link between structural dynamics at early time scales (e.g. early edge ruffling dynamics triggered by stretch onset[19]) and adaptation time scales (adaptation of SF orientation) has not been established. Mathematical models that describe stretch-induced SF reorientation are based on the premise that changes in cytoskeletal tension due to periodic matrix stretch is sufficient to cause disassembly of SFs whose level of extension is perturbed

from a set-point level.[16] SF disassembly begins within minutes after onset of cyclic stretch by a process that is accelerated in SFs experiencing the greatest amplitude of stretch. SF reassembly occurs preferentially in the direction of minimum stretch, resulting in the accumulation of SFs perpendicular to the stretch axis.[16] Whether cycles of spatially polarized edge ruffling contribute to contractility-modulated SF self-adjustment and subsequent reorientation remains unclear.

Although cell edge protrusions perpendicular to the stretch axis are increased over a time scale of hours during cell alignment,[7] quantitative measurements of edge ruffling dynamics at shorter time scales more relevant to mechanosignaling events are lacking. This study tested the hypothesis that dynamic, directional edge ruffling is a prerequisite for SF reorientation in response to cyclic uniaxial stretch. By measuring the degree and orientations of actin edge ruffling in confluent aortic ECs, we show that onset of either cyclic uniaxial or equibiaxial stretch (12%, 1 Hz) caused an increase in edge ruffling that was initially non-directional. After 60 min of stretch, edge ruffling orientations were concentrated perpendicular to the stretch axis, consistent with the eventual SF alignment direction. Rho-kinase (ROCK) inhibition caused edge ruffling orientations to concentrate parallel to the stretch axis after 60 min, remaining correlated with the eventual SF alignment direction. Inhibition of actin-related protein-2/3 (Arp2/3) attenuated cell elongation, disrupted polarized edge dynamics, and inhibited microtubule organizing center (MTOC) reorientation. However, Arp2/3 inhibition had a negligible effect on SF reorientation perpendicular to the stretch axis. Taken together, these results suggest that directional edge ruffling is not a determining factor of SF reorientation in response to stretch. Furthermore, disrupting localization of the Rac effector p21-activated kinase (PAK) had no effect on the extent of stretch-induced SF reorientation, suggesting that PAK is not critical in regulating cytoskeletal remodeling in response to substrate stretch.

Materials and Methods

Cell culture, transfection, and inhibitors

Bovine aortic ECs were maintained in Dulbecco's Modified Eagle Medium (DMEM, Gibco, Gaithersburg, MD) supplemented with 10% heat-inactivated newborn calf serum (HyClone, Logan, UT), 2.92 mg/ml L-glutamine (Gibco), 50 u/ml penicillin (Gibco), and 50 μg/ml streptomycin (Gibco) using established techniques.[12] Cells were transiently transfected with pEGFP-actin (Clontech, Mountain View, CA) using a liposome-mediated method according to manufacturer's recommendations (Lipofectin, Invitrogen, Carlsbad, CA). After 24 h, transfected cells were seeded onto a sterilized elastic membrane coated for 2 h with 1.2 $\mu g/cm^2$ fibronectin (Sigma-Aldrich, St. Louis, MO). Fluorescent microspheres (0.1 μm, Molecular Probes, Eugene, OR) that were pre-adhered by drying on the elastic membrane prior to fibronectin coating were used for image registration and to measure the imposed substrate strain. In experiments using the Rho-kinase inhibitor Y27632 (Calbiochem), cells were pretreated for 30 min, and Y27632 (10 μM) was present throughout the experiment. In experiments using the Arp2/3 complex inhibitor CK-869 (Calbiochem) or its inactive control compound CK-312 (Calbiochem), cells were pretreated for 2 h, and either CK-869 or CK-312 (10 μM) remained present throughout the experiment. To inhibit PAK, cells were

pretreated with a cell-permeant inhibitory peptide that corresponds to the Nck-binding sequence of PAK or a control peptide[27] (20 μg/ml; kind gifts from A.W. Orr, LSU Health Sciences Center) for 1 h, and the peptides were present throughout the experiment.

Stretch application and live-cell image acquisition

Cells were subjected to mechanical stretch using a custom-built device as described previously.[19] The stretch device was enclosed in an Okolab microscope cage incubator (Warner Instruments, Hamden, CT) and maintained at 37 °C and 5% CO_2. In cyclic stretch experiments the indenter motion was sinusoidal (12% linear stretch, 1 Hz), and time-lapse images of ECs expressing EGFP-actin were acquired every 3 min through a 40×/0.75 NA objective lens (Olympus, Center Valley, PA) using a DeltaVision RT Restoration Microscope (Applied Precision, Issaquah, WA) and a cooled CCD camera (MicroMax, Princeton Instruments, Trenton, NJ). The elastic membrane was held at the stretched position for ~30 s during acquisition of multi-wavelength 3-D image stacks (3–4 optical sections spaced 300 nm apart for registration in the *z*-axis). The motion profile was immediately restarted after image acquisition. Acquired images were deconvolved in *softWoRx* software (Applied Precision) using a constrained iterative algorithm and an experimentally measured point spread function[14] and exported in TIFF format. Constant-intensity background subtraction and unsharp mask filtering were performed.

Immunofluorescence

ECs were fixed with 4% paraformaldehyde in PBS and permeabilized with 0.2% Triton X-100 in PBS. To measure SF orientations, F-actin was labeled with TRITC-phalloidin (Sigma). To determine the location of the MTOC, cells were labeled with an antibody against γ-tubulin (Sigma) followed by Cy3-conjugated IgG (Sigma). Cell nuclei were counterstained with bisBenzimide (Hoechst 33258, Sigma). Samples were imaged using a 40×/0.75 NA objective lens as described above.

Image analysis of edge dynamics

We implemented an image analysis strategy that measures the spatiotemporal distribution of actin edge ruffling.[20] Briefly, time-lapse images of ECs expressing EGFP-actin were segmented using an active contour method. In intensity line profiles oriented normal to the cell edge, peak detection identified the angular distribution of polymerized actin within 3 μm of the cell edge, which was localized to lamellipodia and edge ruffles. Edge features associated with filopodia and peripheral SFs were removed. To enable analysis of multiple cells with varying perimeter lengths, cell edge coordinates were grouped based on the polar angle with respect to the centroid position (angular bin size = 1°). To capture dynamic ruffling edges in time, locations of sustained ruffling (angular bins positive for ruffling in at least 3 out of 5 frames) were found using a temporal accumulator.

A nonparametric circular statistics approach[5] was used to assess edge ruffling orientations. In individual ECs, angular distributions of edge ruffles detected by image analysis were represented as unit vectors on the circle with vector angles θ_i ($i = 1 \ldots N$) and used to compute the mean resultant length and the mean orientation angle. The Rayleigh test was used to assess whether edge ruffles were uniformly distributed or were concentrated around

a unimodal direction. If the null hypothesis of uniform distribution was rejected, edge ruffling activity was considered directional with a mean ruffling orientation of $\bar{\theta}$. To compare directionality in multiple cells, mean ruffling orientations of individual ECs $\bar{\theta}_j$ (j = 1…M), where M = number of cells, were then represented as unit vectors on the circle and used to compute a sample mean resultant length and sample mean orientation. Before stretch and during cyclic equibiaxial stretch, the Rayleigh test was used to assess uniformity against a unimodal alternative with unspecified mean direction. During cyclic uniaxial stretch, it was hypothesized that stretch-induced edge ruffles concentrate around the eventual SF alignment direction.[7] The modified Rayleigh test (v-test) was used to test uniformity against a specified, hypothetical unimodal alternative that was set as either perpendicular (90°) or parallel (0°, in the presence of Y27632) to the stretch axis. For measures of spread (i.e. circular variance), axial data were transformed to vector data for analysis.

In computing the mean ruffling orientation in single ECs, we assumed that stretch-induced edge ruffling distribution was either unimodal or unimodal axial ($\bar{\theta}$ and $\bar{\theta}$+180°). To distinguish between these two possibilities a method of moments estimation[5] was used to determine whether the distribution could be fitted as a mixture of two von Mises distributions: component 1 with proportion p, mean orientation μ_1, concentration κ_1, and component 2 with proportion 1 p, mean orientation μ_2, concentration κ_2. Estimates of the five parameters were found by minimizing the least squares criterion at a specified tolerance for convergence.[22] Edge ruffling distributions were considered unimodal axial if $0.75>p>0.25$ and $|\mu_1 - \mu_2|>135°$ (within 45° of a true unimodal axial distribution). As p approaches 1 or 0, the choice of distribution has less effect on the analysis. Mean orientation was not computed for cells with low edge activity (sustained ruffling detected in <10% of the perimeter).

Image analysis of SF orientations

From acquired images of F-actin, local filament orientations were computed from the pixel-by-pixel gradient vector.[23] The 1024×1024-pixel SF image was divided into 64×64-pixel subimages, and the horizontal and vertical gradient in pixel intensity in each subimage I was computed using Sobel operators h_x = [−1 −2 −1; 0 0 0; 1 2 1] and $h_y = h_x'$. Each kernel was convolved with I: $G_x = (h_x * I)$, $G_y = (h_y * I)$. The gradient magnitude G and direction Φ were computed as $G = (G_x^2+G_y^2)^{1/2}$ and $\Phi = \tan^{-1}(G_y/G_x)$. The local direction of orientation φ was found perpendicular to the intensity gradient Φ. Local filament orientations φ_i (i = 1…N), where N = number of subimages with unimodal axial SF orientation, were then represented as unit vectors on the circle and used to compute the mean SF orientation in a field of view. Axial data were transformed to vector data, and the modified Rayleigh test (v-test) was used to test uniformity against a specified, hypothetical unimodal alternative that was set as perpendicular (90°) to the stretch axis.

MTOC polarity and nucleus orientation

MTOC position was determined by finding the local maximum intensity of γ-tubulin fluorescence in the perinuclear region, and its orientation relative to the geometric center of the nucleus was computed. For nucleus orientation, cell nucleus contour determined by Hoechst staining was fit to an ellipse, and the angle between the major axis of the ellipse and

the stretch axis was computed. Both MTOC orientation with respect to the nucleus and nucleus orientation with respect to the stretch axis were converted to the interval [0°, 90°] and grouped (angular bin size = 30°).

Results

Actin edge ruffling dynamics in response to cyclic stretch

We have shown qualitatively that onset of either cyclic uniaxial or equibiaxial stretch causes an increase in edge ruffling in ECs within minutes,[19] but spatiotemporal dynamics of stretch-induced edge activity on this early time scale have not been characterized. In this study we implemented an image analysis strategy[20] to measure the degree and orientation of edge ruffling in response to cyclic stretch. Time-lapse images of ECs expressing EGFP-actin in a confluent monolayer were acquired every 3 min before and after onset of either cyclic uniaxial or equibiaxial stretch. Ruffling edges were defined as locations on the perimeter with polymerized actin within 3 μm of the cell edge, as indicated by concentrated EGFP-actin fluorescence (Fig. 1). Substrate stretch triggered a rapid increase in edge ruffling, as indicated by the cyan perimeter contour segments and the length of angular bins in corresponding rose plots (Fig. 2A, B, also see Supplemental Movies 1, 2). To quantify the degree of ruffling, the fraction of perimeter engaged in ruffling was computed as the ratio of the number of angular bins engaged in ruffling to the total number of angular bins and averaged over a 15-min measurement window. Mean ruffling perimeter fraction computed across multiple cells shows that edge ruffling was increased after 15 min of either cyclic uniaxial or equibiaxial stretch compared to no-stretch ($p < 0.05$, t-test) (Fig. 2C). The stretch-induced increase in edge activity was sustained over the 30- and 60-min measurement windows. The mean projected cell area derived from EGFP-actin fluorescence remained constant over 60 min in response to either cyclic stretch profile (data not shown).

Mean ruffling orientations in single ECs over corresponding measurement windows were computed from angular distributions of sustained ruffling activity (Fig. 1B, C). These orientations were then represented as unit vectors and used to compute a sample circular variance and mean orientation across multiple cells (Fig. 2D, E). Before stretch, mean ruffling orientations of individual ECs were uniformly distributed ($p > 0.05$, Rayleigh test, assuming distribution is not multimodal) (Fig. 2D, E, $t = 0$ min). Cyclic stretch increased mean ruffling perimeter fraction by ~10% but mean ruffling orientations initially remained uniformly distributed, indicating that the initial ruffling response to stretch was non-directional. After 60 min of uniaxial stretch, mean ruffling orientations were not uniformly distributed and were concentrated perpendicular to the stretch axis ($p < 0.05$, v-test, unimodal alternative of 90°) (Fig. 2D). In contrast, mean ruffling orientations of ECs subjected to equibiaxial stretch remained uniformly distributed during the first 60 min of stretch (Fig. 2E).

A change in stress fiber orientations coincided with a change in edge ruffling orientations

When the Rho pathway is intact, cyclic uniaxial stretch induces perpendicular alignment of SFs. Inhibition of the Rho effector ROCK attenuates SF formation in ECs and causes SFs to form parallel to the stretch axis in response to cyclic stretch.[25,28] To test the hypothesis that

directional edge ruffling is a prerequisite for SF reorientation, we measured edge ruffling in ECs treated with the ROCK inhibitor Y27632. ECs were pretreated for 30 min with 10 μM Y27632 and subjected to cyclic uniaxial stretch for up to 4 h in the presence of the inhibitor. Phalloidin labeling revealed that while cortical F-actin began to reorient parallel to the stretch axis after 1 h, F-actin in the cell interior remained diffuse (Fig. 3C). After 4 h SF content was increased, and these newly formed filaments were aligned parallel to the stretch axis (Fig. 3D) consistent with previous reports.[25,28] The degree of cell shape alignment parallel to the stretch axis was less pronounced than SF alignment (data not shown).

ROCK inhibition decreased the effect of cyclic stretch on the degree of edge ruffling, as demonstrated by time-lapse images of an EGFP-actin–expressing EC subjected to cyclic uniaxial stretch in the presence of Y27632 (Fig. 4A, also see Supplemental Movie 3). While some ECs showed increased ruffling in response to stretch onset, mean ruffling perimeter fractions measured at time intervals before and during the first 60 min of stretch remained constant (Fig. 4B). Similar to untreated cells, mean ruffling orientations of ECs treated with Y27632 were uniformly distributed on the circle before and initially after stretch (Fig. 4C). However, after 60 min mean ruffling directions became concentrated parallel to the stretch axis ($p < 0.05$, v-test, unimodal alternative of 0°), in agreement with the eventual SF alignment direction. Thus, our results suggest that a change in edge ruffling orientations after 60 min corresponds to the change in SF orientations observed after 4 h.

Arp2/3 inhibition disrupted stretch-induced directional ruffling but not perpendicular alignment of stress fibers

To determine whether spatially polarized edge dynamics is a primary mechanism guiding cytoskeletal alignment, we intervened against actin filament nucleation at cell edges using CK-869, a small molecule inhibitor of Arp2/3 complex.[36] First, the inhibitor assay was validated by examining the effect of Arp2/3 inhibition on cell shape and actin structures in subconfluent ECs, where edge ruffling activity is more pronounced. Subconfluent ECs were maintained in low (0.5%) serum for 14–16 h and treated with Arp2/3 inhibitor CK-869 (10 or 20 μM) or its inactive control compound CK-312 (20 μM). Low serum conditions were chosen to reduce baseline edge ruffling activity that may be caused by serum components such as platelet-derived growth factor and lysophosphatidic acid. Cell morphology was not noticeably perturbed after a 2 h incubation with the inactive control, and phalloidin labeling showed higher intensity staining in edge ruffles. In contrast, ECs treated with either 10 or 20 μM of Arp2/3 inhibitor adopted a rounded morphology without detaching from the substrate (Fig. 5A). Contrast changes observed in both brightfield and fluorescence images suggest that cell thickness was increased in the perinuclear region and decreased at cell edges. Additionally, Arp2/3 inhibition decreased F-actin content in edge ruffles, as indicated by decreased intensity and uniform distribution of F-actin staining of edge ruffles (Fig. 5B, C). These measurements on subconfluent ECs under no-stretch conditions validate the effectiveness of Arp2/3 inhibition.

In order to measure stretch-induced edge ruffling dynamics in a confluent monolayer of ECs, cells were first pretreated with the Arp2/3 inhibitor or its inactive control (both 10 μM, 2 h pretreatment) and then were subjected to cyclic uniaxial stretch in the presence of the

compounds (Fig. 6). The effect of Arp2/3 inhibition on a confluent monolayer of ECs was more gradual than on a subconfluent cell layer. ECs in a confluent monolayer exhibited a rounded morphology after pretreatment with the Arp2/3 inhibitor, whereas confluent EC monolayers pretreated with the inactive control did not show altered morphology. Although the degree of cell elongation was reduced by Arp2/3 inhibition, image analysis of EGFP-actin dynamics showed that actin polymerization at cell edges was not prevented completely. Dynamic ruffling edges associated with concentrated EGFP fluorescence were detected in cells treated with either the inactive control (Fig. 6A, $t = 0$ min) or the Arp2/3 inhibitor (Fig. 6B, $t = 0$ min; also see Supplemental Movies 4, 5) and the mean ruffling perimeter fraction was not different between the two groups (Fig. 6C, $t = 0$ min).

After onset of cyclic uniaxial stretch, EGFP-actin dynamics reflected a difference in edge ruffling behaviors (Fig. 6, $t > 0$ min). In ECs treated with the inactive control, cyclic stretch onset induced a transient increase in non-directional edge ruffling that was observed at 15 min ($p < 0.05$, t-test) (Fig. 6C). After 60 min, mean ruffling perimeter fraction was not different from the no-stretch baseline; however, mean ruffling orientations were not uniformly distributed but were concentrated perpendicular to the stretch axis ($p < 0.05$, v-test, unimodal alternative of 90°) (Fig. 6D). In contrast, when Arp2/3 was inhibited mean ruffling perimeter fraction remained constant before and during the first 60 min of cyclic stretch (Fig. 6C). While stretch application triggered an increase in edge ruffling in some cells, a synchronized response was not observed. After 60 min, edge activity remained variable among individual cells. In some cases, portions of the perimeter remained dynamic even though edge displacement was reduced. Visually, these dynamic edges did not exhibit a characteristic convex shape with a concentrated band of polymerized actin that is normally associated with edge protrusions. In other cases, attenuation of actin assembly at cell edges was more pronounced and only cortical actin associated with quiescent edges remained. Furthermore, Arp2/3 inhibition disrupted directional edge ruffling in response to stretch, since mean ruffling orientations of ECs treated with Arp2/3 inhibitor were uniformly distributed on the circle before and during the first 60 min of cyclic stretch (Fig. 6E). At the 60-min measurement window, edge activity in 33% (6 out of 18) of the cells was non-directional (angular distribution of sustained edge ruffles was neither unimodal nor unimodal axial). This was caused in part by cells with quiescent edges and a low degree of sustained edge activity, from which mean orientations could not be computed.

To determine whether polymerized actin at cell edges coincided with edge protrusions, the projected cell area derived from EGFP-actin fluorescence was tracked. Relative area change in regions parallel and perpendicular to the stretch axis (quadrants designated “ends” and “sides”, respectively) between $t = 15$–60 min of cyclic stretch was compared (Fig. 7A). In cells treated with the inactive control, projected area decreased at cell ends and relative area change was significantly different from that at cell sides ($p < 0.05$, t-test). In contrast, when Arp2/3 was inhibited, projected area remained relatively unchanged and no difference was observed between cell ends and sides (Fig. 7B). Furthermore, while the magnitude of relative area change computed over a 15-min window was small, orientations of projected area growth in cells treated with the inactive control concentrated perpendicular to the stretch axis after 60 min ($p < 0.05$, v-test, unimodal alternative of 90°) consistent with that

of detected edge ruffles. Directionally polarized edge extensions as indicated by projected area growth was disrupted when Arp2/3 was inhibited (Fig. 7C). These data suggest that polymerized actin at cell edges was not associated with directional edge extensions in the presence of Arp2/3 inhibitor.

We next assessed whether Arp2/3 inhibition affects stretch-induced SF reorientation. In cells treated with the inactive control, cyclic uniaxial stretch induced perpendicular reorientation of SFs after 2 h concomitant with cell elongation (Fig. 8A, B). Treatment with Arp2/3 inhibitor did not prevent SF assembly, as SFs were observed in no-stretch control cells after 5 h of treatment with the inhibitor (Fig. 8C). While Arp2/3 inhibition attenuated stretch-induced cell elongation and ECs retained a rounded morphology, central SFs in stretched cells still reoriented perpendicular to the stretch axis (Fig. 8D, E). To quantify the extent of SF reorientation, filament orientations were first computed locally from the gradient vector in 64×64-pixel subimages. Local filament orientations were then used to compute the mean SF orientation across multiple fields of view. In cells treated with either Arp2/3 inhibitor or its inactive control, mean SF orientations were concentrated perpendicular to the stretch axis (inactive control: mean orientation = −87.7°, circular variance = 0.12; Arp2/3 inhibitor: mean orientation = −89.1°, circular variance = 0.05). The non-parametric Watson U^2 test was used to test the hypothesis that SF orientations in the two groups are drawn from the same population. At the 0.05 significance level, the null hypothesis (H_0: the two samples are drawn from the same population) could not be rejected, suggesting that across the monolayer Arp2/3 inhibition had no effect on the extent of stretch-induced SF reorientation. Since inhibiting Arp2/3 disrupted polarized edge dynamics but not the extent of SF reorientation, edge ruffling is unlikely to be a primary mechanism that guides SF reorientation in response to stretch.

While central SFs were aligned perpendicular to the stretch axis, we observed thick cortical F-actin bundles in ECs treated with Arp2/3 inhibitor that did not reorient perpendicular to stretch and contributed to the rounded cell morphology (Fig. 8D, arrowheads). This difference in F-actin structure at cell edges accounted for the subtle differences between the circular histograms computed across multiple fields of view (Fig. 8A, 8D, rose plots, increased lengths of angular bins between 0°–30° and 150°–180°). We further investigated this effect by computing the circular variance of local F-actin orientations within individual fields of view, which accentuated the contribution of individual F-actin bundles. At this smaller length scale, Arp2/3 inhibition caused an increase in median circular variance of F-actin orientations ($p < 0.05$, Wilcoxon rank-sum test compared to inactive control) (Fig. 8F). Thus, the increased variance of local filament orientations within individual fields of view reflected a change in cell shape (attenuated cell elongation due to Arp2/3 inhibition). Across the monolayer, the overall F-actin orientation is dominated by central SFs, whose force-induced reorientation response was not affected by Arp2/3 inhibition.

Arp2/3 inhibition disrupted stretch-induced MTOC polarization and attenuated nucleus reorientation

Arp2/3 inhibition attenuated cell elongation but did not prevent SF reorientation to stretch, resulting in the decoupling of cell shape and cytoskeletal polarity. To further examine the

effects of Arp2/3 inhibition on stretch-induced cell polarization, we measured MTOC position relative to the nucleus, an indicator of planar cell polarity. Confluent ECs pretreated with Arp2/3 inhibitor or its inactive control were subjected to cyclic uniaxial stretch in the presence of the compounds. After 4 h of uniaxial stretch, ECs treated with the inactive control were elongated and reoriented perpendicular to the stretch axis, whereas the degree of cell elongation remained reduced in ECs treated with the inhibitor (Fig. 9A). To assess MTOC polarity, cells were labeled with anti-γ-tubulin and counterstained for cell nuclei (Fig. 9B). MTOC orientation relative to the nucleus (θ) was scored as perpendicular to the stretch axis if $60° < \theta \leq 90°$ (stretch axis = 0°). For ECs treated with the inactive control and subjected to stretch, the fraction of cells with MTOC perpendicular to the stretch axis was different from 0.33 (random distribution), suggesting a bias in MTOC orientations ($p < 0.05$ compared to a mean of 0.33, t-test). In contrast, MTOC polarization was not observed in cells treated with the inhibitor or in cells kept as no-stretch control (Fig. 9C). Moreover, the fraction of cells with polarized MTOC was greater in cells stretched in the presence of the inactive control compared to other groups ($p < 0.05$, ANOVA and post hoc multiple comparison test). These results suggest that Arp2/3 inhibition disrupted stretch-induced MTOC polarization.

Shear stress causes nucleus shape alignment in the flow direction in addition to SF reorientation and MTOC polarization.[6] To determine whether nucleus alignment occurs in response to stretch, cell nucleus contours were fitted to an ellipse, and the angle between the major axis of the ellipse and the stretch axis was computed. Nucleus orientation (θ) was scored as perpendicular to the stretch axis if $60° < \theta \leq 90°$ (stretch axis = 0°). Perpendicular reorientation of nuclei in response to stretch was observed in cells treated with either the Arp2/3 inhibitor or its inactive control, suggesting that Arp2/3 inhibition did not prevent nucleus orientation to stretch ($p < 0.05$ compared to a mean of 0.33, t-test) (Fig. 9D). In contrast, nuclei were randomly oriented in cells kept as no-stretch control. Comparing across groups showed that the fraction of cells with polarized nuclei was greater in cells stretched in the presence of the inactive control compared to other groups ($p < 0.05$, ANOVA and post-hoc multiple comparison test). Thus, while Arp2/3 inhibition did not prevent nucleus reorientation, the degree of polarization was decreased. Although static uniaxial stretch caused elongation of the nucleus in a previous study,[2] we did not observe a change in nuclear eccentricity after 4 h of cyclic stretch (data not shown).

PAK inhibition did not prevent stretch-induced stress fiber reorientation

Blocking polarized Rac activity inhibits static stretch-induced SF reorientation in subconfluent smooth muscle cells,[24] suggesting that Rac may regulate stretch-induced SF reorientation similar to that in response to shear stress.[42] Furthermore, shear stress stimulates activation of the Rac effector PAK in ECs cultured on fibronectin,[37] and expression of dominant negative PAK blocks shear stress-induced SF reorientation.[1] Based on these observations, we hypothesized that PAK mediates SF reorientation in confluent ECs exposed to cyclic uniaxial stretch. To test the role of PAK in stretch-induced SF reorientation, ECs were maintained in 0.5% serum for 14–16 h, pretreated for 1 h with a cell-permeant PAK-Nck inhibitory peptide or a control peptide[27] (20 μg/ml) and subjected to cyclic uniaxial stretch for 4 h in the presence of the peptides. The PAK-Nck peptide has

been shown previously to inhibit PAK function similarly to full length dominant negative constructs by preventing PAK translocation to sites of action such as cell-cell junctions. This inhibition of PAK activation was sufficient to inhibit its effects on EC migration, contractility, and permeability.[27,37,38]

In cells treated with either the PAK-Nck peptide or the control peptide, SFs reoriented perpendicular to the stretch axis (Fig. 10A, B) (Control peptide: mean orientation = 86.8°, circular variance = 0.03; PAK-Nck peptide: mean orientation = 89.3°, circular variance = 0.04). The Watson U^2 test was used to test the hypothesis that SF orientations in the two groups are drawn from the same population. At the 0.05 significance level, the null hypothesis (H_0: the two samples are drawn from the same population) could not be rejected, suggesting that PAK inhibition had no effect on the extent of stretch-induced SF reorientation measured in multiple fields of view across the monolayer. Furthermore, median circular variance of local filament orientations measured within individual fields of view was not different in cells treated with the PAK-Nck peptide and the control peptide (Fig. 10C). These data suggest that PAK binding to Nck and subsequent localization is not a critical step in stretch-induced SF reorientation.

Discussion

In ECs, cytoskeletal alignment and directionally polarized cell motility are important adaptive responses to directional mechanical cues such as unidirectional shear stress and cyclic uniaxial stretch. However, mechanisms controlling cell polarization are not fully understood. It has been hypothesized that flow-mediated directional ruffling facilitates EC polarization and subsequent migration through positive feedback loops comprised of integrin signaling, Rac-mediated actin polymerization, and microtubule elongation at the leading edge. At the cell rear, Rho-mediated contractility and focal adhesion (FA) disassembly promote detachment from the substrate.[30] Thus, analogous to the cell migration paradigm, spatial asymmetry of actin polymerization at cell edges may represent the first step in establishing planar cell polarity in response to mechanical cues. Force-induced polarization mechanisms in confluent monolayers are less clear, as the magnitude of shear stress-induced edge ruffling is lower and ruffling orientations remain non-directional after 15 min.[34] Furthermore, other rapid shear stress-induced structural changes such as strain focusing in the intermediate filament network[13] and downstream displacement of FA sites and ECM fibrils[34] appear to be transient over this time scale. Most intermediate filament displacement occurs within the first few minutes after flow onset, and over 15 min displacement patterns of subcellular structures become more heterogeneous. In contrast, significant cytoskeletal alignment[6] and persistent migration[31] in the flow direction is not observed until >10 h after flow onset. Thus, there exists a gap in knowledge on whether structural changes at early time scales such as actin edge ruffling is a prerequisite for long-term force-mediated structural adaptation.

Cell shape and SF reorientation represent common functional readouts of cell adaptation to cyclic stretch. However, few studies have measured rapid structural changes that may be involved in mechanosignaling and directional sensing. In this study, we implemented an image analysis strategy to measure the degree and orientations of actin edge ruffling in

response to cyclic stretch. Our results show that cyclic stretch onset induced an increase in actin edge ruffling in confluent ECs. The initial (<15 min) response to stretch occurred in a non-directional manner, similar to the effect of shear stress in both subconfluent and confluent ECs.[34] Moreover, increased edge ruffling was observed in response to either uniaxial or equibiaxial stretch. These results support the hypothesis that mechanical force onset represents a depolarizing signal that resets cell polarity,[44] regardless of whether the stimulus is directional. Consistent with this hypothesis, human aortic ECs subjected to cyclic stretch first adopt a rounded morphology, which occurs after initial SF disassembly and precedes cell elongation perpendicular to the stretch axis.[35] Although cyclic stretch-induced edge ruffling is initially non-directional, a unimodal mean ruffling orientation perpendicular to the stretch axis emerges after 60 min. It has been demonstrated using kymography that the average number of edge protrusions perpendicular to stretch increases over 3 h as cells aligned.[7] Here, we show at higher spatial and temporal resolution that directional edge activity likely precedes complete cell and SF reorientation. Measuring actin edge dynamics may therefore provide a tool that is predictive of shape alignment for investigating molecular mechanisms.

Rho signaling and Rho-mediated cell contractility play important roles in determining the orientation response to stretch. Specifically, inhibiting Rho or Rho effectors such as ROCK, mDia, or myosin light chain kinase (MLCK) attenuates SF formation but causes stretch-induced SF assembly oriented parallel to the stretch axis.[25,28] These previous results provide a means to test the spatial correlation between edge ruffling and SF orientations. In ECs treated with ROCK inhibitor Y27632, mean ruffling perimeter fraction remained constant before and during the first 60 min of cyclic stretch. Since ROCK antagonizes Rac activation,[41] its inhibition may cause an increase in constitutive edge ruffling activity and thereby mask the effect of cyclic stretch. Similar to non-treated ECs, edge ruffling during cyclic stretch was initially non-directional in the presence of Y27632. After 60 min, edge ruffles concentrated parallel to the stretch axis in the direction of eventual SF alignment. These data suggest that a change in SF orientations caused by ROCK inhibition coincides with a change in edge ruffling orientations, and the two remain spatially correlated. Our observation that F-actin remained diffuse in the cytoplasm after 60 min further supports a temporal relationship in which polarized edge dynamics may guide SF reorientation to stretch. Rho activity modulates actin-myosin contractility and cytoskeletal tension. It has been hypothesized that inhibiting Rho signaling prevented an increase in actin dynamics, and consequently SFs aligned passively in the direction of stretch.[3] A change in edge ruffling orientations could be a reflection of this altered contractile state, but the functional significance remains unclear.

The Arp2/3 complex controls the assembly of actin filaments into dendritic networks at the leading edge of motile cells.[8] We initially hypothesized that if edge ruffling is a determining factor of SF reorientation in response to stretch, disruption of spatially polarized actin edge activity through Arp2/3 inhibition would attenuate SF alignment. Actin filament nucleation at cell edges was perturbed pharmacologically using CK-869, a small molecule inhibitor of Arp2/3 complex that inserts into the hydrophobic core of Arp3 and alters its conformation.[36] Pretreatment with Arp2/3 inhibitor CK-869 (10 μM) induced a rounded morphology in ECs after 2 h, consistent with previous observations in fibroblasts.[40] Actin polymerization near

cell edges was still observed, likely due to remaining Arp2/3 activity (IC_{50} = 11 μM against bovine Arp2/3 [36]). However, phalloidin labeling showed that F-actin content in edge ruffles was decreased compared to cells treated with the inactive control CK-312. In ECs expressing EGFP-actin and treated with Arp2/3 inhibitor, mean ruffling perimeter fraction remained constant before and during the first 60 min of cyclic stretch. However, the variability of both edge ruffling magnitude and orientation among individual ECs was increased after stretch onset. CK-869 causes mislocalization of Arp3 and N-WASP in wound-edge fibroblasts.[40] In those cells, colocalization of Arp3, N-WASP, and actin was reduced at the leading edge and became more spatially heterogeneous. Our observation of reduced and randomly oriented actin edge dynamics is consistent with those results. After 60 min of cyclic stretch, 66% (12 out of 18) of the cells exhibited directional ruffling, but compiled across multiple cells these mean ruffling orientations remained spatially uniform. By comparing relative changes in projected cell area and orientations of projected area growth (both derived from cell contours), we further demonstrate that Arp2/3 inhibition disrupted polarized edge extensions.

In cells treated with Arp2/3 inhibitor, the angular distribution of mean SF orientations measured across multiple fields of view was not different from that in cells treated with the inactive control, suggesting that inhibiting Arp2/3 had no effect on the extent of stretch-induced SF reorientation. Instead, Arp2/3 inhibition increased circular variance of local filament orientations measured in subimages within individual fields of view. This increased variability could be attributed to thick F-actin bundles at cell edges, which did not align due to the inability of cells to elongate in response to stretch. Taken together, image analysis of F-actin orientations at different length scales suggests that stretch-induced remodeling of cortical and central SFs may involve distinct mechanisms. These results are consistent with previous work showing that dorsal SFs (assembled through formin-driven actin polymerization at FAs) are distinct from transverse arcs (that originated from the lamellipodial network and consisted of cortical Arp2/3-nucleated actin bundles).[15] Similar differences in peripheral vs. central SF reorganization have also been reported in stretched ECs treated with inhibitors of ROCK or MLCK.[28] In those cells, cyclic uniaxial stretch cause SFs to form parallel to the stretch axis. However, SFs in ECs treated with Y27632 are primarily located near cell-cell junctions, whereas SFs in ECs treated with MLCK inhibitor ML-7 are confined to central regions of the cell.[28] Spatial asymmetry of actin polymerization in response to external cues guides the establishment of planar cell polarity. In motile cells, this is accompanied by redistribution of the MTOC to the leading edge.[10] In ECs subjected to shear stress, microtubule dynamics is required for polarized edge protrusions and subsequent migration in the flow direction.[18] Likewise in response to cyclic stretch, migration of fibroblasts perpendicular to the stretch axis was blocked by treatment with either nocodazole or taxol.[7] However, disruption or stabilization of microtubules did not block cell and SF reorientation in response to cyclic stretch.[7,43] Our observation that directional edge ruffling in response to cyclic stretch is not a determining factor of SF reorientation provides further evidence that cytoskeletal remodeling and cell motility may be independently regulated despite their spatially correlated orientations. Stretched ECs treated with Arp2/3 inhibitor retained a rounded morphology but exhibited SFs aligned perpendicular to the stretch axis. Decoupling of cell shape and cytoskeletal alignment in

response to stretch has been previously reported in smooth muscle cells, where inhibition of stretch-activated cation channels suppressed perpendicular reorientation of cell shape but not SFs.[11] Similarly, stretch causes perpendicular alignment of SFs in focal adhesion kinase (FAK) -null mouse embryonic fibroblasts, but cell elongation is attenuated.[17] These observations support the hypothesis that stretch-induced cell shape and SF remodeling involve distinct signaling pathways. Interestingly, inhibition of FAK phosphorylation has been shown to block stretch-induced EC migration in addition to elongation.[46] While we did not measure migration in this study, reduced elongation and impaired wound healing was observed in fibroblasts treated with CK-869.[40] Collectively, these data further suggest that directional motility in response to stretch is not mediated by SF reorientation, and the two processes are likely independently regulated.

To further examine the effects of Arp2/3 inhibition on stretch-induced cell polarization, we measured MTOC position relative to the nucleus, an indicator of planar cell polarity. Cyclic stretch causes redistribution of the MTOC to the elongated side of the cytoplasm perpendicular to the stretch axis after 24 h.[21] Consistently, we observed cell elongation and a bias in MTOC distribution perpendicular to the stretch axis after 4 h in cells treated with the inactive control. Arp2/3 inhibition attenuated stretch-induced cell elongation and disrupted MTOC polarization, suggesting that although stretch-induced SF reorientation remained unaffected some aspects of planar cell polarity (including cell shape and MTOC polarization) were suppressed. The functional significance of these effects remains uncertain. MTOC polarization in wound-edge fibroblasts is not dependent on actin, Arp2/3, or WASP-family proteins.[32] Specifically, delocalization of Arp2/3 by overexpression of Scar1-WCA does not affect MTOC polarization in wound-edge cells.[32] This discrepancy may be due to asymmetries in cell-cell contact formed by the scratch wound (i.e. the presence of a free cell edge). Furthermore, MTOC reorientation occurs by rearward movement of the nucleus away from the leading edge in a process that is coupled with actin retrograde flow and during which the MTOC remains stationary at the cell centroid.[9] We reason that since Arp2/3 inhibition attenuated cell elongation and shape polarization, nucleus movement as an initial polarizing event may be suppressed in the absence of an established leading edge or an elongated side. Consequently, MTOC polarization in these cells was blocked or delayed. Our observation of decreased nucleus reorientation perpendicular to the stretch axis in cells treated with Arp2/3 inhibitor further supports a role for Arp2/3 in nucleus movement.

Since Rac is upstream of SF reorientation in response to both flow and stretch,[24,42] and since flow-mediated SF reorientation is blocked by expression of a dominant negative construct of the Rac effector PAK,[1] we further tested whether PAK, an important regulator of EC contractility,[26,38] mediates stretch-induced SF reorientation. Incubation with a cell-permeant PAK-Nck inhibitory peptide, which in previous studies inhibited EC migration and angiogenesis,[27,37] did not prevent SF reorientation perpendicular to the stretch axis and had no effect on the extent of stretch-induced SF remodeling. These results suggest that despite its role in promoting EC motility, PAK may not be critical in regulating cytoskeletal remodeling in response to substrate stretch.

Overall, it is important that inhibiting directional edge ruffling in response to uniaxial stretch did not prevent SF alignment. Thus, a potential mechanism is ruled out: the original hypothesis that early polarization of actin-mediated ruffling is required for SF adaptation is false. As a result, the causal links between early Rac-mediated cytoskeletal dynamics and Rho-mediated cellular adaptations to mechanical stimuli remain elusive.

Supplementary Material

Refer to Web version on PubMed Central for supplementary material.

Acknowledgments

The authors thank A. Wayne Orr for the generous gift of Nck-binding PAK peptides and Martin Schwartz for valuable discussions. Supported by NIH Grant HL080956 and by a University of Virginia VPRGS Award.

Abbreviations

EC	endothelial cell
SF	stress fiber
Arp2/3	actin-related protein-2/3
MTOC	microtubule organizing center

References

1. Birukov KG, Birukova AA, Dudek SM, Verin AD, Crow MT, Zhan X, DePaola N, Garcia JG. Shear stress-mediated cytoskeletal remodeling and cortactin translocation in pulmonary endothelial cells. Am J Respir Cell Mol Biol. 2002; 26:453–464. [PubMed: 11919082]
2. Caille N, Tardy Y, Meister JJ. Assessment of strain field in endothelial cells subjected to uniaxial deformation of their substrate. Ann Biomed Eng. 1998; 26:409–416. [PubMed: 9570224]
3. Chien S. Mechanotransduction and endothelial cell homeostasis: The wisdom of the cell. Am J Physiol Heart Circ Physiol. 2007; 292:H1209–1224. [PubMed: 17098825]
4. Choi CK, Helmke BP. Short-term shear stress induces rapid actin dynamics in living endothelial cells. Mol Cell Biomech. 2008; 5:247–258. [PubMed: 20084179]
5. Fisher, N. Statistical analysis of circular data. Cambridge University Press; 1993.
6. Galbraith CG, Skalak R, Chien S. Shear stress induces spatial reorganization of the endothelial cell cytoskeleton. Cell Motil Cytoskeleton. 1998; 40:317–330. [PubMed: 9712262]
7. Goldyn AM, Rioja BA, Spatz JP, Ballestrem C, Kemkemer R. Force-induced cell polarisation is linked to rhoa-driven microtubule-independent focal-adhesion sliding. J Cell Sci. 2009; 122:3644–3651. [PubMed: 19812308]
8. Goley ED, Welch MD. The arp2/3 complex: An actin nucleator comes of age. Nat Rev Mol Cell Biol. 2006; 7:713–726. [PubMed: 16990851]
9. Gomes ER, Jani S, Gundersen GG. Nuclear movement regulated by cdc42, mrck, myosin, and actin flow establishes mtoc polarization in migrating cells. Cell. 2005; 121:451–463. [PubMed: 15882626]
10. Gotlieb AI, May LM, Subrahmanyan L, Kalnins VI. Distribution of microtubule organizing centers in migrating sheets of endothelial cells. J Cell Biol. 1981; 91:589–594. [PubMed: 7309800]
11. Hayakawa K, Sato N, Obinata T. Dynamic reorientation of cultured cells and stress fibers under mechanical stress from periodic stretching. Exp Cell Res. 2001; 268:104–114. [PubMed: 11461123]

12. Helmke BP, Goldman RD, Davies PF. Rapid displacement of vimentin intermediate filaments in living endothelial cells exposed to flow. Circ Res. 2000; 86:745–752. [PubMed: 10764407]
13. Helmke BP, Rosen AB, Davies PF. Mapping mechanical strain of an endogenous cytoskeletal network in living endothelial cells. Biophys J. 2003; 84:2691–2699. [PubMed: 12668477]
14. Hiraoka Y, Sedat JW, Agard DA. Determination of three-dimensional imaging properties of a light microscope system. Partial confocal behavior in epifluorescence microscopy. Biophys J. 1990; 57:325–333. [PubMed: 2317554]
15. Hotulainen P, Lappalainen P. Stress fibers are generated by two distinct actin assembly mechanisms in motile cells. J Cell Biol. 2006; 173:383–394. [PubMed: 16651381]
16. Hsu HJ, Lee CF, Kaunas R. A dynamic stochastic model of frequency-dependent stress fiber alignment induced by cyclic stretch. PLoS One. 2009; 4:e4853. [PubMed: 19319193]
17. Hsu HJ, Lee CF, Locke A, Vanderzyl SQ, Kaunas R. Stretch-induced stress fiber remodeling and the activations of jnk and erk depend on mechanical strain rate, but not fak. PLoS One. 5:2010.
18. Hu YL, Li S, Miao H, Tsou TC, del Pozo MA, Chien S. Roles of microtubule dynamics and small gtpase rac in endothelial cell migration and lamellipodium formation under flow. J Vasc Res. 2002; 39:465–476. [PubMed: 12566972]
19. Huang L, Mathieu PS, Helmke BP. A stretching device for high-resolution live-cell imaging. Ann Biomed Eng. 2010; 38:1728–1740. [PubMed: 20195762]
20. Huang L, Helmke BP. A semi-automatic method for image analysis of edge dynamics in living cells. Cell Mol Bioeng. 2011; 4:205–219. [PubMed: 21643526]
21. Iba T, Sumpio BE. Morphological response of human endothelial cells subjected to cyclic strain in vitro. Microvasc Res. 1991; 42:245–254. [PubMed: 1779881]
22. Jones TA. Matlab functions to analyze directional (azimuthal) data--i: Single-sample inference. Computers & Geosciences. 2006; 32:166.
23. Karlon WJ, Hsu PP, Li S, Chien S, McCulloch AD, Omens JH. Measurement of orientation and distribution of cellular alignment and cytoskeletal organization. Ann Biomed Eng. 1999; 27:712–720. [PubMed: 10625144]
24. Katsumi A, Milanini J, Kiosses WB, del Pozo MA, Kaunas R, Chien S, Hahn KM, Schwartz MA. Effects of cell tension on the small gtpase rac. J Cell Biol. 2002; 158:153–164. [PubMed: 12105187]
25. Kaunas R, Nguyen P, Usami S, Chien S. Cooperative effects of rho and mechanical stretch on stress fiber organization. Proc Natl Acad Sci U S A. 2005; 102:15895–15900. [PubMed: 16247009]
26. Kiosses WB, Daniels RH, Otey C, Bokoch GM, Schwartz MA. A role for p21-activated kinase in endothelial cell migration. J Cell Biol. 1999; 147:831–844. [PubMed: 10562284]
27. Kiosses WB, Hood J, Yang S, Gerritsen ME, Cheresh DA, Alderson N, Schwartz MA. A dominant-negative p65 pak peptide inhibits angiogenesis. Circ Res. 2002; 90:697–702. [PubMed: 11934838]
28. Lee CF, Haase C, Deguchi S, Kaunas R. Cyclic stretch-induced stress fiber dynamics - dependence on strain rate, rho-kinase and mlck. Biochem Biophys Res Commun. 2010
29. Li S, Butler P, Wang Y, Hu Y, Han DC, Usami S, Guan JL, Chien S. The role of the dynamics of focal adhesion kinase in the mechanotaxis of endothelial cells. Proc Natl Acad Sci U S A. 2002; 99:3546–3551. [PubMed: 11891289]
30. Li S, Huang NF, Hsu S. Mechanotransduction in endothelial cell migration. J Cell Biochem. 2005; 96:1110–1126. [PubMed: 16167340]
31. Lin X, Helmke BP. Micropatterned structural control suppresses mechanotaxis of endothelial cells. Biophys J. 2008; 95:3066–3078. [PubMed: 18586851]
32. Magdalena J, Millard TH, Machesky LM. Microtubule involvement in nih 3t3 golgi and mtoc polarity establishment. J Cell Sci. 2003; 116:743–756. [PubMed: 12538774]
33. Matsumoto T, Yung YC, Fischbach C, Kong HJ, Nakaoka R, Mooney DJ. Mechanical strain regulates endothelial cell patterning in vitro. Tissue Eng. 2007; 13:207–217. [PubMed: 17518594]
34. Mott RE, Helmke BP. Mapping the dynamics of shear stress-induced structural changes in endothelial cells. Am J Physiol Cell Physiol. 2007; 293:C1616–1626. [PubMed: 17855768]

35. Ngu H, Feng Y, Lu L, Oswald SJ, Longmore GD, Yin FC. Effect of focal adhesion proteins on endothelial cell adhesion, motility and orientation response to cyclic strain. Ann Biomed Eng. 2010; 38:208–222. [PubMed: 19856213]

36. Nolen BJ, Tomasevic N, Russell A, Pierce DW, Jia Z, McCormick CD, Hartman J, Sakowicz R, Pollard TD. Characterization of two classes of small molecule inhibitors of arp2/3 complex. Nature. 2009; 460:1031–1034. [PubMed: 19648907]

37. Orr AW, Stockton R, Simmers MB, Sanders JM, Sarembock IJ, Blackman BR, Schwartz MA. Matrix-specific p21-activated kinase activation regulates vascular permeability in atherogenesis. J Cell Biol. 2007; 176:719–727. [PubMed: 17312022]

38. Stockton RA, Schaefer E, Schwartz MA. P21-activated kinase regulates endothelial permeability through modulation of contractility. J Biol Chem. 2004; 279:46621–46630. [PubMed: 15333633]

39. Sumpio BE. Hemodynamic forces and the biology of the endothelium: Signal transduction pathways in endothelial cells subjected to physical forces in vitro. J Vasc Surg. 1991; 13:744–746. [PubMed: 2027223]

40. To C, Shilton BH, Di Guglielmo GM. Synthetic triterpenoids target the arp2/3 complex and inhibit branched actin polymerization. J Biol Chem. 2010; 285:27944–27957. [PubMed: 20566646]

41. Tsuji T, Ishizaki T, Okamoto M, Higashida C, Kimura K, Furuyashiki T, Arakawa Y, Birge RB, Nakamoto T, Hirai H, Narumiya S. Rock and mdia1 antagonize in rho-dependent rac activation in swiss 3t3 fibroblasts. J Cell Biol. 2002; 157:819–830. [PubMed: 12021256]

42. Tzima E, Del Pozo MA, Kiosses WB, Mohamed SA, Li S, Chien S, Schwartz MA. Activation of rac1 by shear stress in endothelial cells mediates both cytoskeletal reorganization and effects on gene expression. Embo J. 2002; 21:6791–6800. [PubMed: 12486000]

43. Wang JH, Goldschmidt-Clermont P, Wille J, Yin FC. Specificity of endothelial cell reorientation in response to cyclic mechanical stretching. J Biomech. 2001; 34:1563–1572. [PubMed: 11716858]

44. Wojciak-Stothard B, Ridley AJ. Shear stress-induced endothelial cell polarization is mediated by rho and rac but not cdc42 or pi 3-kinases. J Cell Biol. 2003; 161:429–439. [PubMed: 12719476]

45. Wootton DM, Ku DN. Fluid mechanics of vascular systems, diseases, and thrombosis. Annu Rev Biomed Eng. 1999; 1:299–329. [PubMed: 11701491]

46. Yano Y, Geibel J, Sumpio BE. Tyrosine phosphorylation of pp125fak and paxillin in aortic endothelial cells induced by mechanical strain. Am J Physiol. 1996; 271:C635–649. [PubMed: 8770005]

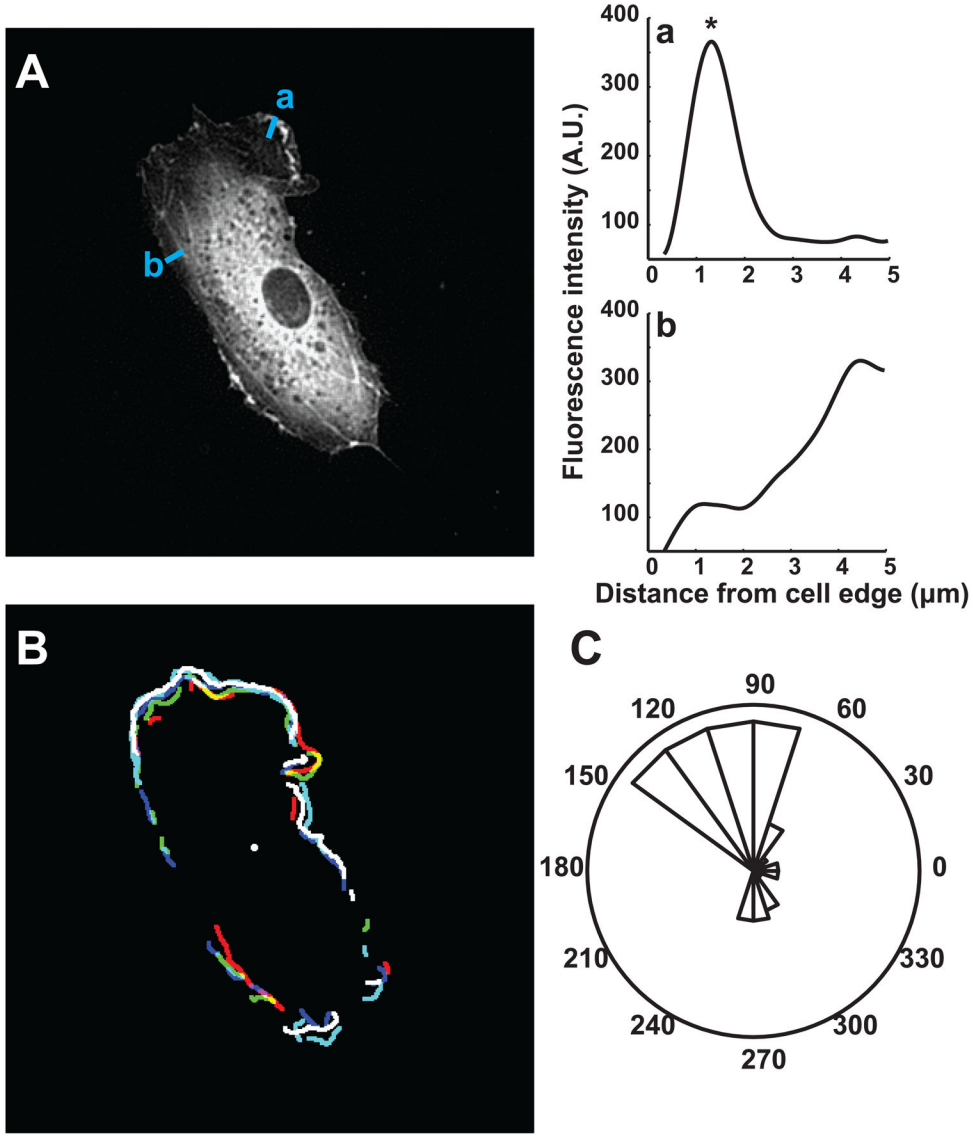

Figure 1.

Spatial and temporal accumulator to detect dynamic ruffling edges. (A) EC expressing EGFP-actin subjected to stretch. (a,b) Representative intensity line profiles normal to the cell edge. Fluorescence intensity peaks detected inside a 3-μm-wide edge region (*) were assigned to ruffles. (B) Overlay of ruffling segments detected by image analysis during a 15-min window. (C) Rose plot shows the angular distribution of sustained ruffle segments (angular bins detected in at least 3 out of 5 frames). Edge ruffling magnitude and orientation were compared across different measurement windows before and after onset of cyclic stretch.

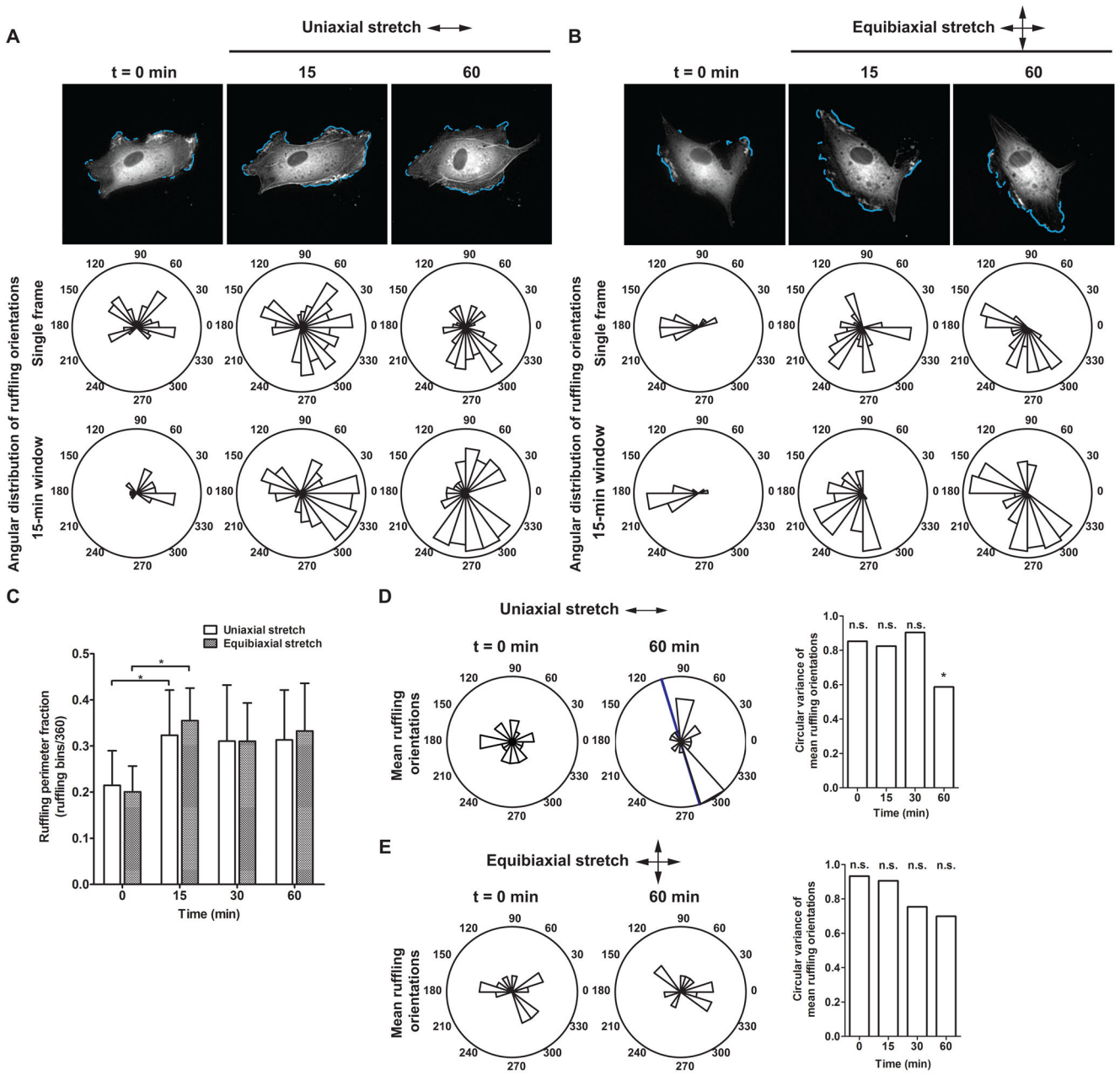

Figure 2.

EGFP-actin dynamics in response to cyclic stretch. (A, B) Time-lapse images of ECs in a confluent monolayer subjected to (A) cyclic uniaxial stretch and (B) cyclic equibiaxial stretch. Rose plots show the angular distribution of edge ruffles in the corresponding image and during a 15-min measurement window. Arrows indicate stretch directions. Scale bars, 20 μm. (C–E) Effect of cyclic stretch on the magnitude and orientation of actin edge ruffling. (C) Mean ruffling perimeter fraction, computed as the ratio of the number of angular bins engaged in ruffling to the total number of angular bins. (*, $p < 0.05$, t-test compared to $t = 0$ min) (D, E) Circular variance computed from the angular distribution of mean ruffling orientations of individual cells. Rose plots show mean ruffling orientations of

individual ECs at indicated times. Blue bar indicates mean ruffling orientation across multiple cells. Arrows indicate stretch directions. (*, $p < 0.05$, v-test, unimodal alternative of 90°) (Uniaxial stretch: $n = 20$ cells; equibiaxial stretch: $n = 14$ cells from separate experiments)

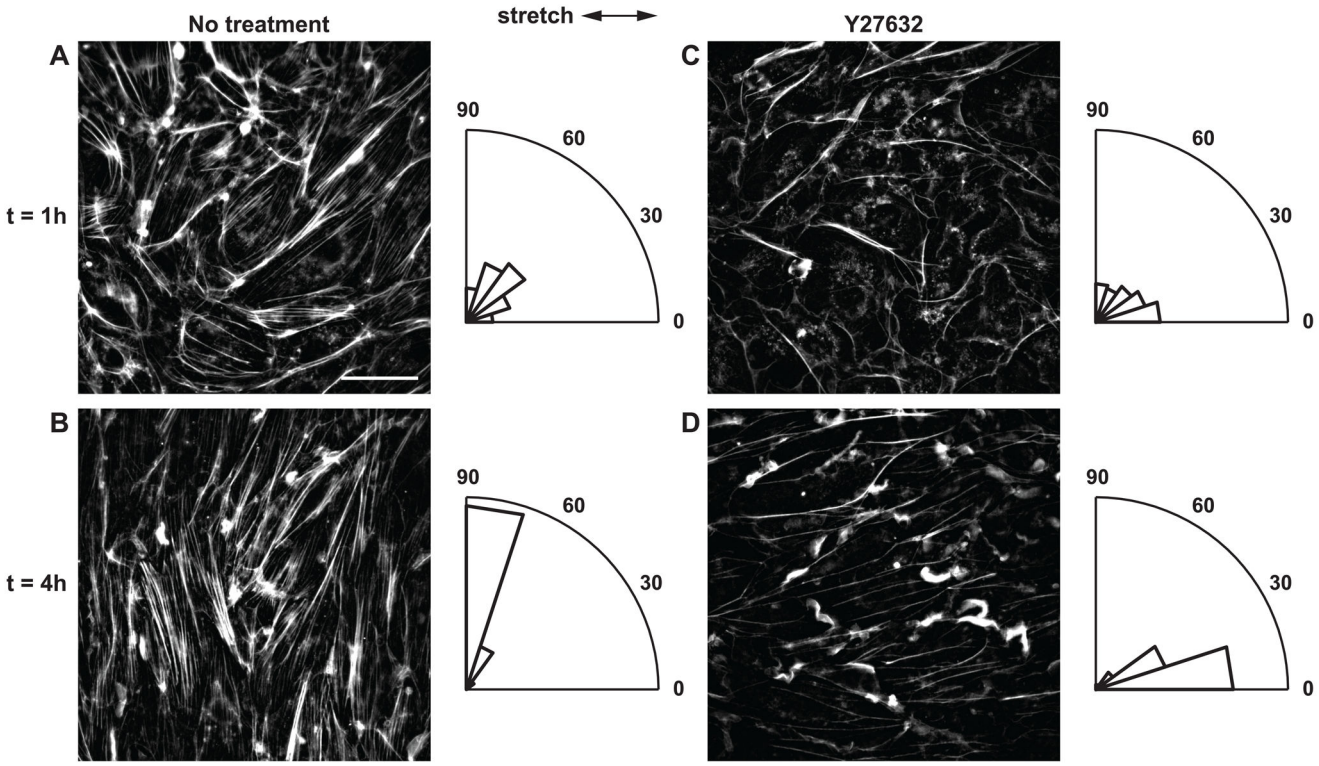

Figure 3.

Effect of ROCK inhibition on stretch-induced SF reorientation. (A, B) Untreated ECs and (C, D) ECs treated with ROCK inhibitor Y27632 were subjected to cyclic uniaxial stretch for up to 4 h. Arrows indicate stretch directions. Scale bar, 20 μm. Rose plots show normalized angular distribution of F-actin orientations of the corresponding image.

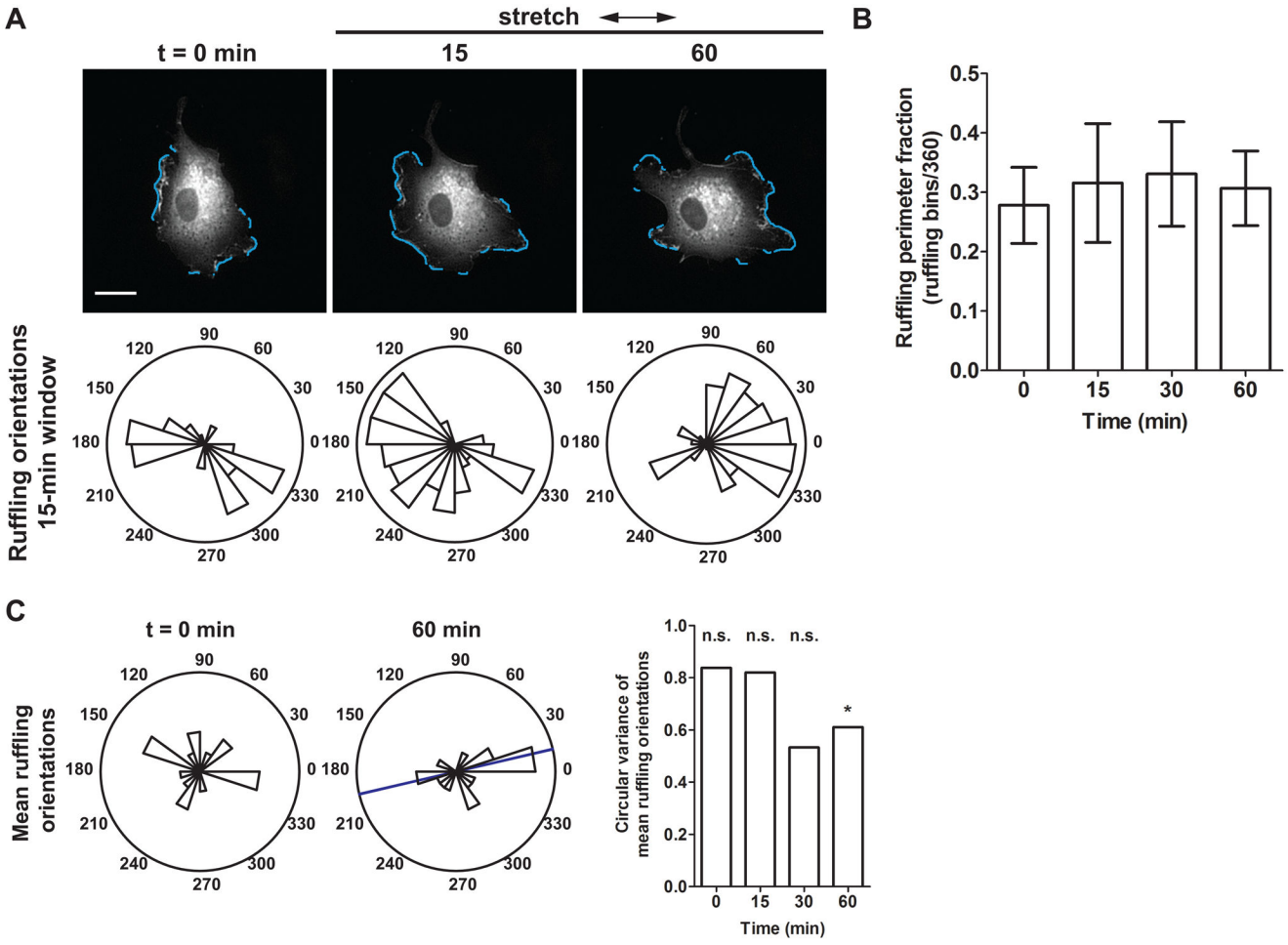

Figure 4.

Effect of ROCK inhibition on stretch-induced edge ruffling. (A) EGFP-actin dynamics in an EC pretreated with Y27632 and subjected to cyclic uniaxial stretch in the presence of the inhibitor. Rose plots show the angular distribution of edge ruffles in during a 15-min measurement window. Arrows indicate stretch directions. Scale bars, 20 μm. (B) Mean ruffling perimeter fraction, computed as the ratio of the number of angular bins engaged in ruffling to the total number of angular bins. (C) Circular variance computed from the angular distribution of mean ruffling orientations of individual cells. Rose plots show mean ruffling orientations of individual ECs at indicated times. Blue bar indicates mean ruffling orientation across multiple cells. (*, $p < 0.05$, v-test, unimodal alternative of 0°) ($n = 17$ cells from separate experiments)

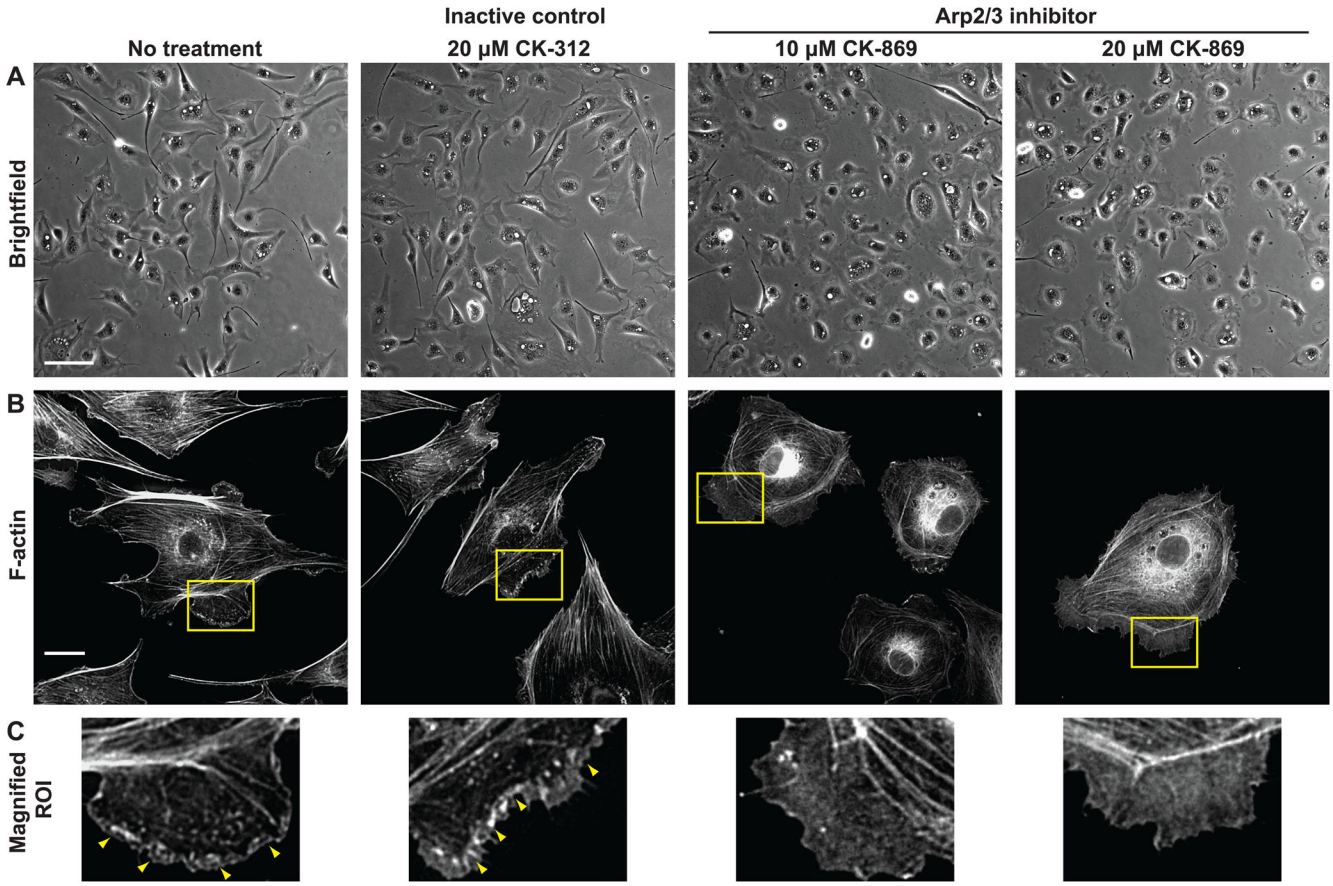

Figure 5.

Effect of Arp2/3 inhibition on EC morphology and F-actin content. (A) Morphology of subconfluent ECs pretreated for 2 h with Arp2/3 complex inhibitor CK-869, inactive control CK-312, or left untreated. Scale bar, 100 μm. (B) F-actin staining. Scale bar, 20 μm. (C) Magnified view of regions of interest indicated by yellow boxes in (B). Arrowheads show higher intensity phalloidin staining in edge ruffles.

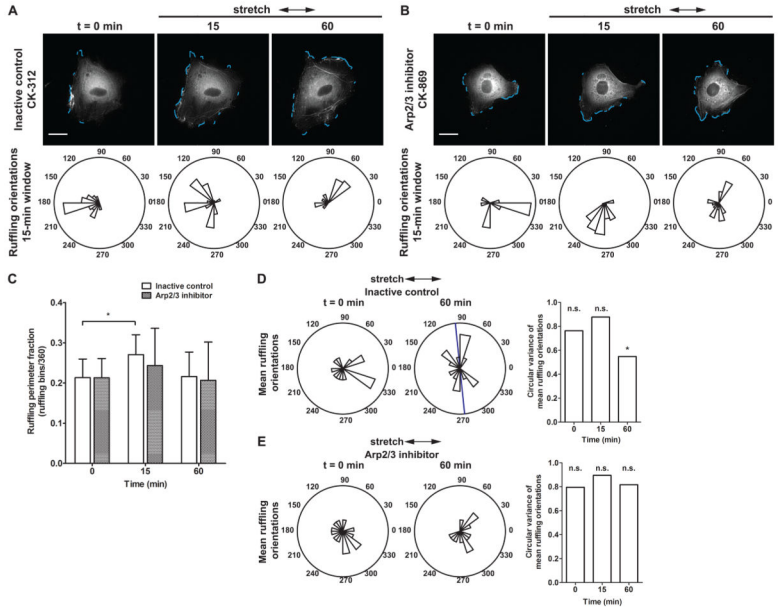

Figure 6.

Effect of Arp2/3 inhibition on stretch-induced edge ruffling. Time-lapse images of ECs pretreated for 2 h with (A) inactive control compound CK-312 or (B) Arp2/3 complex inhibitor CK-869 and subjected to cyclic uniaxial stretch in the presence of the compounds. Rose plots show the angular distribution of edge ruffles in during a 15-min measurement window. Arrows indicate stretch directions. Scale bars, 20 μm. (C) Mean ruffling perimeter fraction, computed as the ratio of the number of angular bins engaged in ruffling to the total number of angular bins. (*, $p < 0.05$, t-test compared to $t = 0$ min) (D, E) Circular variance computed from the angular distribution of mean ruffling orientations of individual cells. Rose plots show mean ruffling orientations of individual ECs at indicated times. Blue bar indicates mean ruffling orientation across multiple cells. (*, $p < 0.05$, v-test, unimodal alternative of 90°) (Inactive control CK-312: $n = 15$; Arp2/3 inhibitor CK-869: $n = 18$ cells cells from separate experiments)

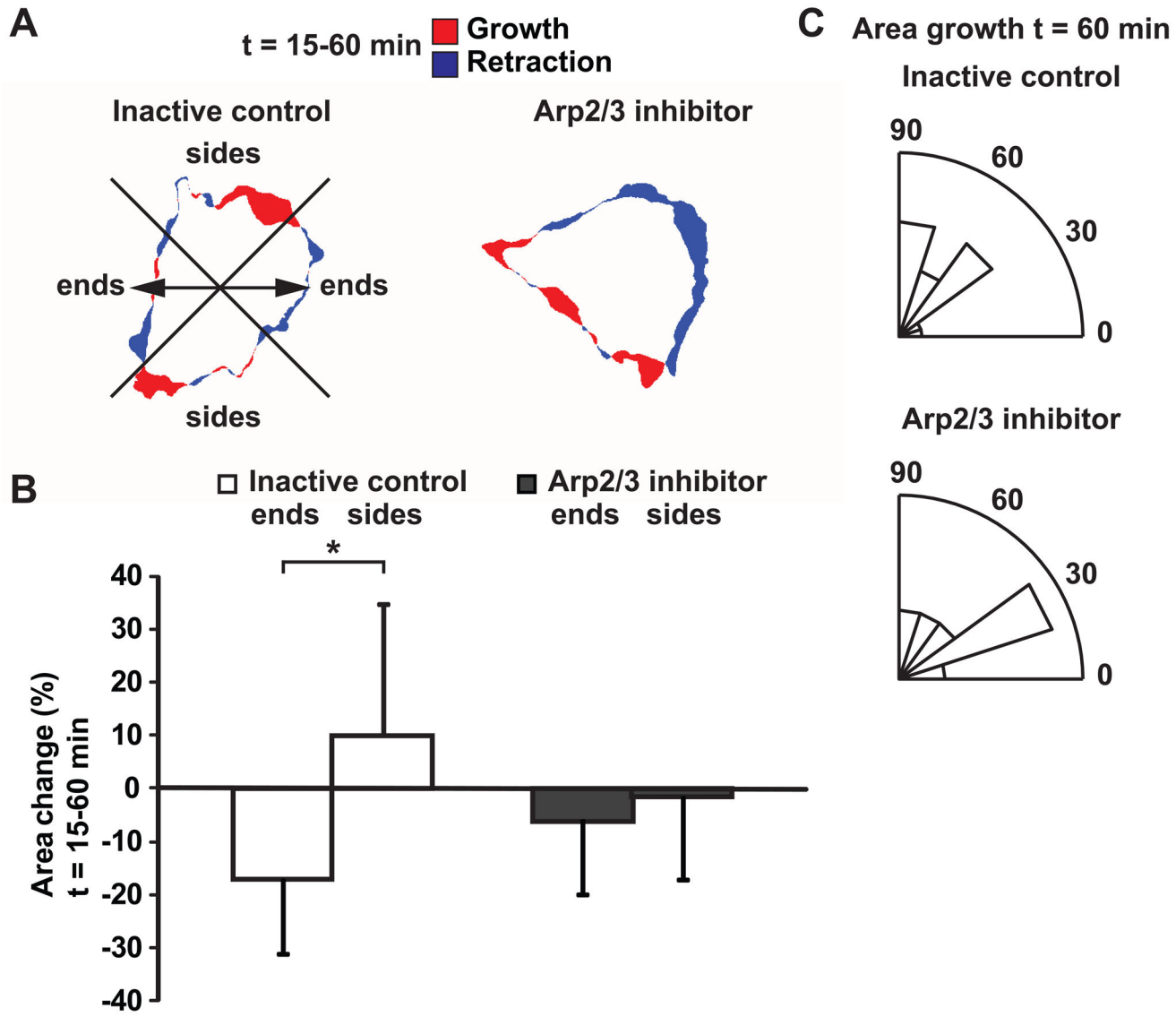

Figure 7.

Effect of Arp2/3 inhibition on stretch-induced change in projected cell area. (A) Change in projected cell area between t = 15–60 min after cyclic stretch onset. Red and blue regions indicate area growth and retraction, respectively. Arrows indicate stretch directions. ECs were pretreated with inactive control CK-312 or Arp2/3 inhibitor CK-869 for 2 h and stretched in the presence of the compounds. (B) Relative change in projected area at cell "ends" parallel to stretch and "sides" perpendicular to stretch. Cells were divided into quadrants with respect to the stretch axis as shown in (A). (*, $p < 0.05$, t-test) (C) Rose plots show angular distribution of projected area growth over a 15-min window at t = 60 min. (Inactive control CK-312: n = 15 cells; Arp2/3 inhibitor CK-869: n = 18 cells from separate experiments)

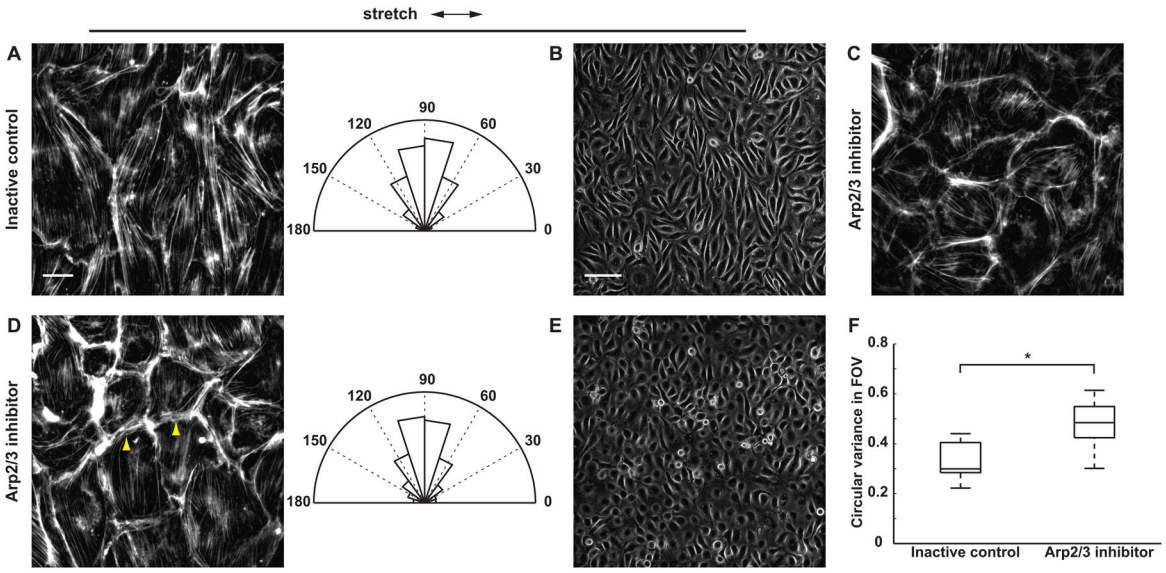

Figure 8.

Effect of Arp2/3 inhibition on stretch-induced SF and cell reorientation. ECs were pretreated with (A, B) inactive control CK-312 or (D, E) Arp2/3 inhibitor CK-869 for 2 h and subjected to cyclic uniaxial stretch for 2 h in the presence of the compounds. Arrowheads show cortical F-actin bundles that did not align to stretch. Rose plots show normalized angular distribution of F-actin orientations computed from the gradient vector in 64×64-pixel subimages (n > 3000 subimages in 15 fields of view in 3 experiments). (C) As control, ECs were treated with Arp2/3 inhibitor for 5 h in the absence of stretch. Arrows indicate stretch directions. Scale bars, F-actin images (A, C, D): 20 μm; brightfield images (B, E): 100 μm. (F) Circular variance of SF orientations within individual fields of view. On each box, central mark: median; edges: 25th and 75th percentiles; whiskers: most extreme data points. (*, p < 0.05, Wilcoxon rank-sum test; n = 15 fields of view in 3 experiments)

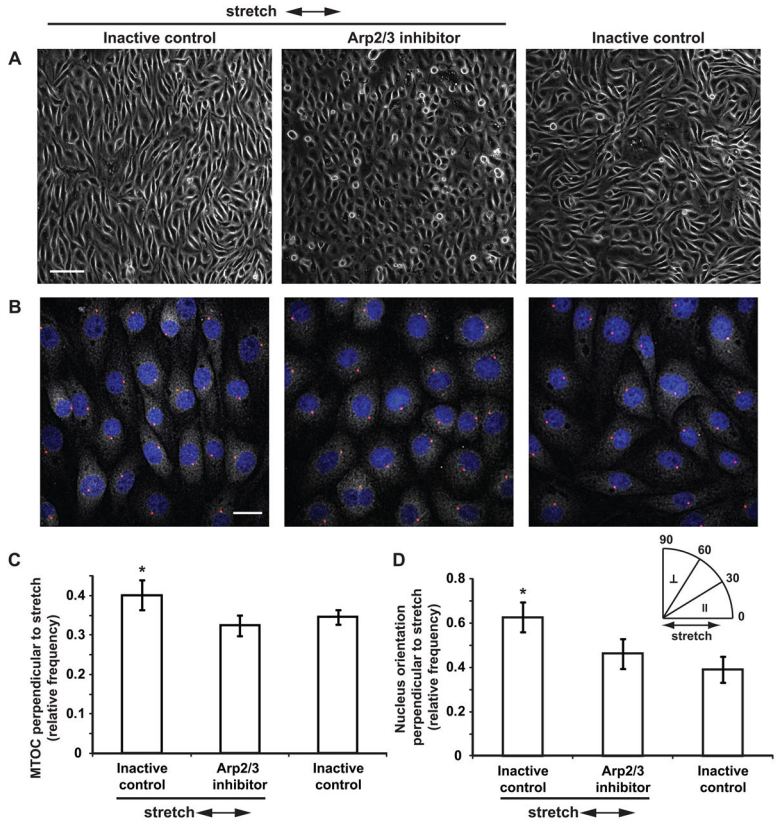

Figure 9.

Effect of Arp2/3 inhibition on stretch-induced MTOC polarization and nucleus reorientation. (A) ECs were pretreated with inactive control CK-312 or Arp2/3 inhibitor CK-869 for 2 h and subjected to cyclic uniaxial stretch for 4 h in the presence of the compounds. Arrows indicate stretch directions. Scale bar, 100 μm. (B) Immunofluorescence staining of γ-tubulin and counterstaining of cell nuclei (blue). Red circles indicate MTOC positions determined from local maximum intensity in the perinuclear region. Scale bar, 20 μm. (C) MTOC polarization. Bars show fraction of cells with MTOC orientation between 60°–90° relative to the nucleus ($60° < \theta \leq 90°$, stretch axis = 0°). (D) Nucleus shape reorientation. Bars show fraction of cells with nucleus orientation between 60°–90° relative to the stretch axis ($60° < \theta \leq 90°$, stretch axis = 0°). Values shown are mean ± standard deviation. ($n \geq 5$ experiments per group; 10 fields of view with ~200 cells per experiment were analyzed. *, $p < 0.05$, ANOVA and multiple comparison test)

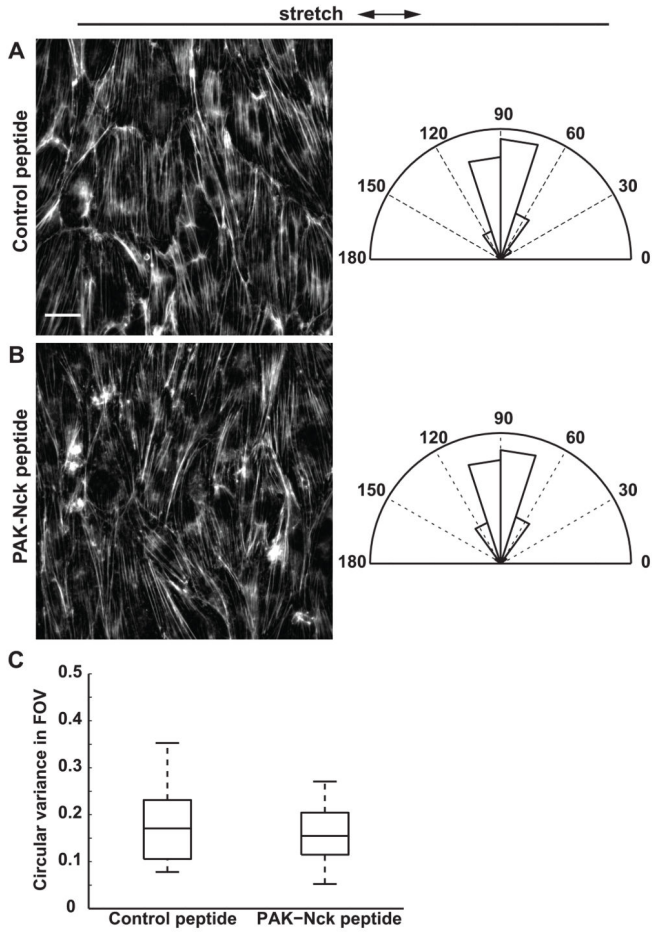

Figure 10.

Effect of PAK inhibition on stretch-induced SF reorientation. (A–B) ECs were pretreated with (A) control peptide or (B) PAK-Nck inhibitory peptide for 1 h and subjected to cyclic uniaxial stretch for 4 h. Arrows indicate stretch directions. Scale bar, 20 μm. Rose plots show normalized angular distribution of F-actin orientations computed in 64×64-pixel subimages (n > 3000 subimages in 15 fields of view in 3 experiments). (C) Circular variance of SF orientations within individual fields of view. On each box, central mark: median; edges: 25th and 75th percentiles; whiskers: most extreme data points. (n = 15 fields of view in 3 experiments)